the two apparent mobilities at any cell depth. Thus if the particle mobilities of unknown samples and the reference sample are measured at the cell center where the migration velocity has a maximum, the real electrophoretic mobility of the unknown sample is given by:

$$U_{el} - U'_{el} = U_{app}(\text{maximum}) - U'_{app}(\text{maximum}) \quad (8)$$

Fig. 1 shows an example indicating the electrophoretic mobility profiles obtained experimentally for the reference sample (PSSNa lattices) and an unknown sample (SM lattices) along the cell depth in a 1×10^{-3} M KCl solution at 25°C. The SM lattices employed as an unknown sample were prepared by the copolymerization of styrene with 5% methacrylic acid (MA) at 70°C. It is apparent that both profiles indicate reasonable parabolical curves, and the curve for the reference lattices shows a constant mobility at the two stationary levels. Furthermore, the difference between the two apparent mobilities at the cell center agrees well with the velocity of the SM lattices at the stationary level.

Fig. 2 shows the ζ-potential vs. pH curves for the SM lattices, which have been determined from the maximum mobilities using the PSSNa lattices as a standard.[6] The same relation obtained from the velocity of the SM lattices at the stationary level is also indicated. As can be seen, both curves agree fairly well over the whole pH range. All of these results indicate that if we have a reliable colloid sample whose ζ-potential is exactly determined, the ζ-potential of the unknown sample can be determined precisely from the measurements of apparent electrophoretic mobility at the cell center. In that case, slight errors in focusing (i.e., errors because of the view field) are less important because the velocity gradient near the level of observation is very small.

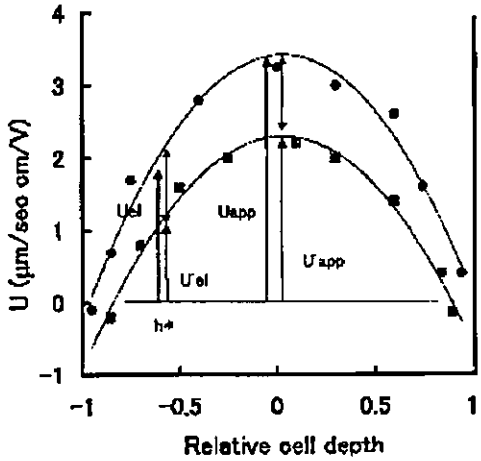

Fig. 1 Examples of electrophoretic mobility profiles of PSSNa lattices (U') and SM lattices (U). (h^*) stationary level; (■) PSSNa lattices; (●) SM lattices (1×10^{-3} M KCl, 25°C).

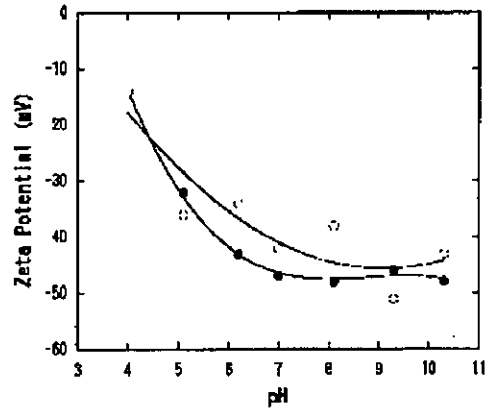

Fig. 2 ζ-Potential vs. pH curves of unknown sample (SM lattices) determined by the maximum velocity of reference sample (●) and the usual method (○).

According to Eqs. 3 and 4, U_0 and hence the ζ-potential of the cell wall are determined using a reference sample. The electroosmotic velocity (U_0) obtained by the extrapolation of the velocity profile to the cell wall permits the determination of the ζ-potential of the cell wall–solution interface, and the ζ-potential measurement of various solid–solution interfaces,[7] including the dissimilar cell system,[8] has been determined. Here, we would like to emphasize again that the determination of the ζ-potential of the cell wall is also possible from the maximum velocity of the reference sample, instead of the tedious plane interface procedure. According to Eq. 4, the apparent velocity of the reference sample at the cell center (at h=0) is $U_{app}' = U_{el}' - U_0'/2$. Therefore U_0' and hence the ζ-potential of the cell wall can be quickly determined if the U_{el}' has been previously known.

Fig. 3 shows some examples of apparent flow velocity profiles of standard latex samples (PSSNa lattices) at various pH values in which both boundaries refer to the glass–solution interface. A symmetrical parabola was given at all pH conditions where the surface charge of glass is consistent with both sides.

ELECTROKINETIC CHARACTERIZATIONS IN CONCENTRATED DISPERSIONS

In recent years, electroacoustics offered studies on surface characterization and the stability of suspended colloid particles. The term electroacoustics refer to two kinds of related phenomena: 1) colloid vibration potential (CVP),

MARCEL DEKKER, INC.
270 Madison Avenue, New York, New York 10016

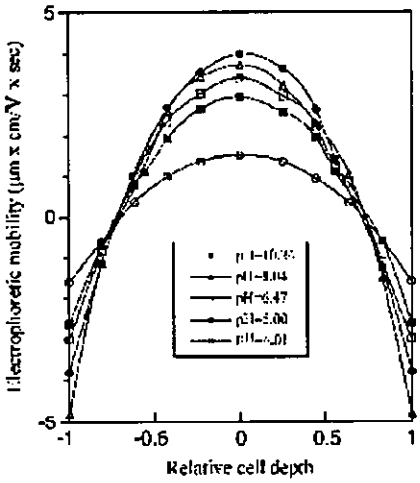

Fig. 3 Apparent flow velocity profile of standard latex samples at various pH values (1×10^{-3} M KCl, 25°C).

in which an electrical field arises in colloidal suspension when a sound wave passes through the dispersion (i.e., ultrasonic vibration causes the difference in movement between charged core particles and countercharges around them, which induces oscillating dipole moments and hence the potential drop in the sample cell);[9] and 2) electrokinetic sonic amplitude (ESA), the reciprocal effect of the above phenomena, in which an alternating electrical field is applied to a suspension and a sound wave arises as a result of the inertia of the particles, caused by their time-alternating electrophoresis (i.e., high-frequency electrical waves cause a difference in movement between the core particles and the countercharges, which generates an ultrasonic waves in the sample cell).[10,11]

A very important advantage of these electroacoustical techniques is their ability to provide accurate measurements of the ζ-potential in concentrated colloid systems. In this section, two of the typical data obtained by these methods are shown.

Surface Characterization of Concentrated Latex Suspensions

In this section, the CVP technique is demonstrated for zeta potential measurements of concentrated suspensions of latex particles with different surface groups.[12] Three types of polystyrene lattices with different surface groups were synthesized in emulsifier-free systems. The usual polystyrene (PSt) lattices were prepared by the method of Kotera et al.,[13] and the two others (PSm and PStn) were synthesized by incorporating small amounts of ionic

Table 2 Characterization of colloid particles

Sample	Diameter (nm)	Surface charge density (μC/cm²) Strong acid	Weak acid	Total
PSt	480	5.3	2.5	7.8
PStn	610	18	0	18
PStm	530	5	33	38

comonomer, methacrylic acid, and sodium polyvinylphenylsulfonate (NaSS) into a polystyrene chain, respectively, as in Juang and Krieger.[14] To increase the particle size, PStn was prepared in a system with 1×10^{-4} mol/dm³ $MgSO_4$. These latex samples were sufficiently dialyzed with distilled water and were then brought into contact with an ion exchange resin to remove ionic impurities. The samples were all composed of highly monodispersed spherical particles with $D_w/D_n = 1.02$, and the surface charge densities of the latex particles were measured by potentiometric and conductometric titration, as in Van den Hul and Vanderhoff.[15] The characterization data of all the samples are summarized in Table 2.

To compare the CVP with the conventional electrokinetic technique, first, the zeta potential of each sample in a dilute state was determined in a 1×10^{-3} mol/dm³ KCl solution at different pH values using the microelectrophoretic technique. The resulting data for four samples are shown in Fig. 4. The ζ-potential of the latex samples, especially the PStn sample, appears to be essentially independent of the medium pH. The zeta potential of PSt increases gradually from acidic to neutral pH. This behavior is probably dependent on the existence of carboxyl groups on the surface (with pK_a values between

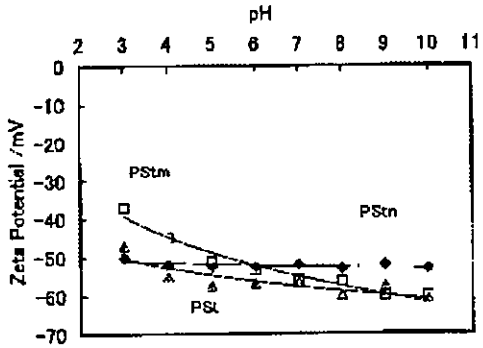

Fig. 4 pH dependence of zeta potential in dilute state measured by the microelectrophoretic technique in 1×10^{-3} mol/dm³ KCl at 25°C.

Marcel Dekker, Inc.
270 Madison Avenue, New York, New York 10016

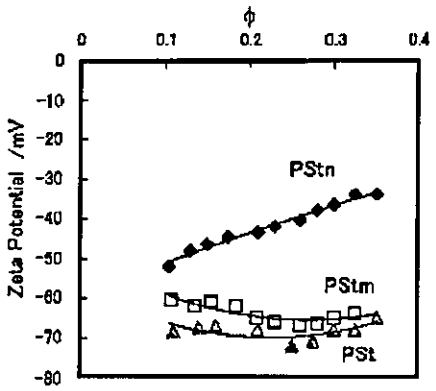

Fig. 5 Concentration dependence of zeta potential for polystyrene latex suspensions in 1×10^{-3} mol/dm^3 KCl at 25°C and pH 5.

about 4 and 5), which are produced by the hydrolysis and subsequent oxidation of the OSO_3^- groups that come from the radical fragments used as an initiator ($K_2S_2O_8$).[16–18]

The CVP measurements of polystyrene lattices give reliable data only in high-volume fraction (ϕ) systems above ϕ=0.1 because the density of the latex particles is small (ρ_2=1.05 g/cm^3) and significant differences of CVP against the background signal can be detected only at high concentration ranges. Figs. 5 and 6 are graphs of the zeta potentials determined by CVP measurements for three kinds of polystyrene lattices at pH 5 and 9, as a function of the ϕ value of each latex. It is apparent that the zeta potentials for PSt and PStm at pH 5 and for PSt at pH 9 have nearly constant values over the entire concentration range of particles, and that the cell model theory is nearly

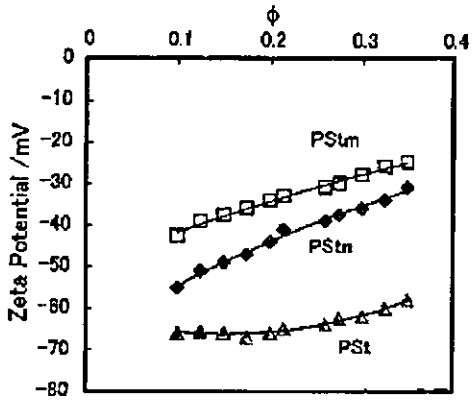

Fig. 6 Concentration dependence of zeta potential for polystyrene latex suspensions in 1×10^{-3} mol/dm^3 KCl at 25°C and pH 9.

valid for those systems. However, the zeta potentials for PStn at pH 5 and for PStn and PStm at both pH values decrease strongly as the particle concentrations increase. Furthermore, it was found that those of PStm at pH 9 are lower than those at pH 5, which is opposite in tendency to those in Fig. 4, determined directly in dilute states by the microelectrophoretic technique. It is thought, from a comparison with Table 2, that this abnormal behavior of the ζ-potential is related to the high surface charge densities of the latex samples (i.e., PStn has many sulfonate groups on the surface brought about by the NaSS component), which dissociate completely under both pH conditions, and PStm becomes covered with thick carboxyl layers coming from the MA molecules, which gradually dissociate as the pH increases. These high surface charge densities bring about an expansion of the surface layer and may cause a double-layer overlapping at moderate particle concentrations, which results in restrictions for the prerequisite of the cell model of Levine et al.[19]

To understand the abnormal behavior of the CVP and ζ-potential that appeared in the latex suspensions, including the particles with high surface charge densities, the concentration dependence of conductivity was measured in the respective systems. The concentration dependence of the conductivity depends largely on the surface nature of the particles.[12] The conductivity of polystyrene latex systems increases as the particle concentration increases. This tendency is especially remarkable in the PStn systems at pH 5 and 9 and in the PStm system at pH 9. From a comparison with the results of the CVP, it was realized that this increasing tendency of the conductivity is closely related to the abnormal behavior of the CVP. This is explained as follows. On the highly charged surfaces of PStn or PStm at pH 9, a polyelectrolyte-like ("hairy") layer is present. These layers overlap each other in this concentrated state, allowing electrical conduction through the hairy layer; thus the hairy layer results in interparticle surface conductance. The degree of interparticle surface conduction is affected by the particle concentration and the thickness of the hairy layer, which in turn depend on the surface charge density of the particle and the pH of the medium.

Application of Electrokinetic Sonic Amplitude Technique in the Ceramic Industry

The concept of colloidal suspension processing has been successfully applied to the field of structural ceramic where inherent properties of dense suspension are used to transform a fluid suspension to a stiff gel. During colloidal processing, the state of dispersion has a significant influence on the casting behavior and the resulting green body properties. The good dispersion of particles

MARCEL DEKKER, INC.
270 Madison Avenue, New York, New York 10016

gives optimum packing state (high green density), which influences the sinterability of the ceramic body and hence the physical and chemical properties of the final product. At present, fine-grained and uniform microstructures are desirable for most ceramic applications in producing strong and reliable structural parts.

Traditionally in the ceramic industry, polyelectrolytes have been utilized to prevent the flocculation of particles. Because of the charged nature of the polyelectrolyte, they impart stability to the particles via an electrosteric mechanism. Hence the adsorption of these charged molecules onto a particle surface will alter the surface charge and hence the zeta potential. Thus using electroacoustics, it is possible to follow the changes in the zeta potential with increasing amounts of polyelectrolyte. This is extremely useful in determining the optimum amount of polyelectrolyte required to stabilize the particles under different conditions.

Fig. 7 shows how the zeta potential of an alumina suspension (background electrolyte, 10 mM KCl) can be altered by the addition of three commercially available polyelectrolytes.[20] Initially, the zeta potential of the suspension is such that the suspension becomes more stable. The trend for all dispersants is very similar in that, initially, the zeta potential changes strongly with small amounts of dispersants and then after a certain concentration, the zeta potential begins to plateau out as no more dispersant is adsorbed on the surface. However, each dispersant imparts a different final zeta potential and requires a different amount of dispersants to cover the particles. Of these, Poly-CA imparts the greatest final zeta potential, so this would be an excellent dispersant for the alumina. However, it must be noted that the likely stabilization mechanism for polyelectrolyte dispersants is electrosteric stabilization. Therefore there may well be a steric contribution to the stabilization mechanism depending on how the dispersant adsorbs. Poly-CE64 imparts a final zeta potential of −45 mV and requires approximately twice as much dispersant to do so, making it a poor candidate in comparison. The zeta potential from the suspension stabilized with Poly-PC 33 does not appear to level out, and further data points would be required to determine the optimum amount.

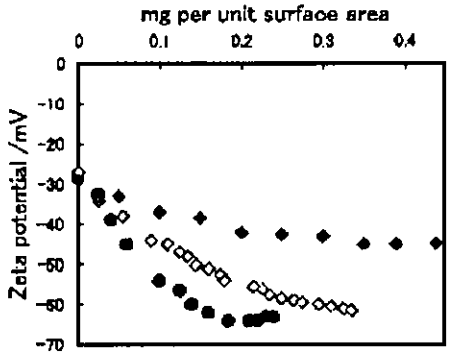

Fig. 7 Effect of three commercial dispersants on alumina suspension in 1×10^{-4} mol/dm^3 KCl: (●) Poly-CA; (◇) Poly-PC33; (◆) Poly-CE64.

ELECTROKINETIC MEASUREMENTS IN SYNTHESIS OF COMPOSITE PARTICLES

There is a variety of methods currently used to fabricate a wide range of stable, composite, and coating particles of various compositions. These include heterocoagulation,[21] seed polymerization,[22] emulsion/phase separation,[23] sacrificial core techniques,[24] and so on. The notion of adsorbing particles onto solid substrates in a layer-by-layer manner was introduced by Iler[25] in the mid-1960s. Decher and Hong[26] extended Iler's work to a combination of linear polycations and polyanions in the early 1990s. Decher[27] later adapted the layer-by-layer technique to include inorganic nanoparticles, biomolecules, clays, and dyes in polyelectrolyte multilayer assemblies. Very recently, Caruso and Mohwald[28] and Caruso et al.[29] reported very interesting results, which included a detailed investigation of the stepwise formation of the silica–nanoparticle/polymer multilayer templating of some latex particles. In this chapter, we demonstrate how we can utilize electrophoretic measurements in synthesis and coating processes of composite particles.

Heterocoagulation Behavior of Polymer Lattices with Spherical Silica

Gherardi and Matijevic[30] have investigated various behaviors of mixed colloid particles obtained by mixing differently preformed particles. They showed that the nature of a mixing system depends on the conditions of preparations, and concluded that the most important parameter in controlling the morphology of composite particles is the surface charge of the component particles, especially the contrast between surface charges of the two component particles. A stable system consisting of a regular composite particle could be prepared only in a medium controlled at a definite pH, where the two components are charged with opposite signs. Typical results

MARCEL DEKKER, INC.
270 Madison Avenue, New York, New York 10016

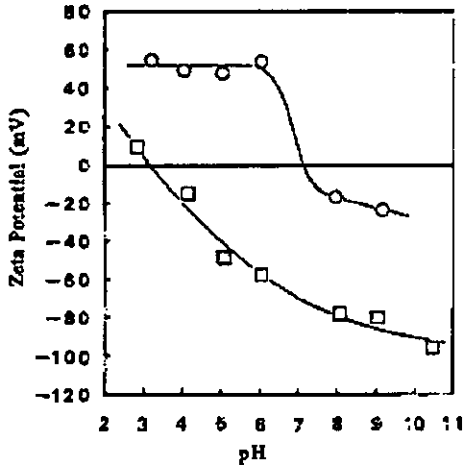

Fig. 8 ζ-Potentials of silica (□) and latex particles (○) as a function of pH at 5×10^{-3} mol/dm^3 KCl.

of the electrophoretic mobility for the single silica and the latex suspension are shown in Fig. 8.

The next important parameter to control morphology is the particle size ratio of the component particles when they are mixed in the vessel. Fig. 9 shows schematic pictures of the morphology of heterocoagulates of different silica particles and amphoteric lattices. Fig. 10 shows an optical micrograph of the real heterocoagulate generated from different silica samples and amphoteric latex systems, where the other conditions (e.g., the particle number ratio, $N_{silica}/N_{latex}=1/300$; medium pH 5.6) have been kept constant. The microscope used for

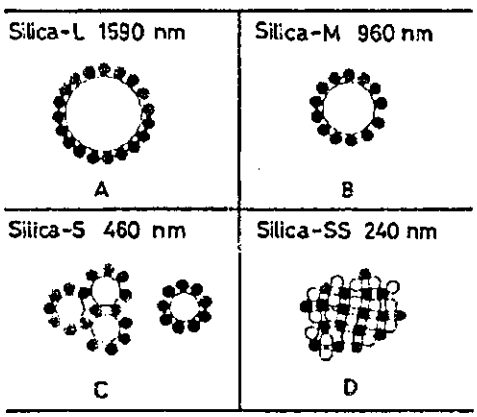

Fig. 9 Schematic pictures showing the morphology of heterocoagulate particles formed from different silica samples.

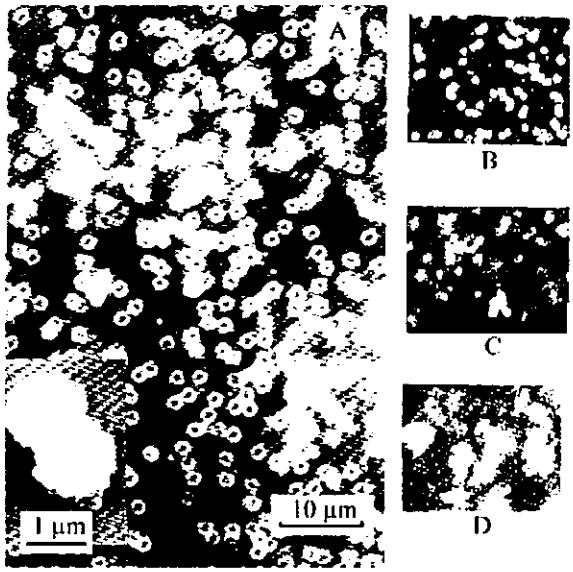

Fig. 10 Optical micrograph showing the heterocoagulates prepared from different silica samples: (A) Silica-L; (B) Silica-M; (C) Silica-S: (D) Silica-SS.

observations was a lateral-type metallurgical microscope (Axio Mart, Carl Zeiss, Germany). It may be seen that at a particle size ratio ($r=D_{silica}/D_{latex}$) higher than 3, the suspension is composed of uniform heterocoagulate particles and each heterocoagulate undergoes Brownian motion as an isolated unit. The insert of Fig. 10A shows a scanning electron micrograph of the heterocoagulate. It

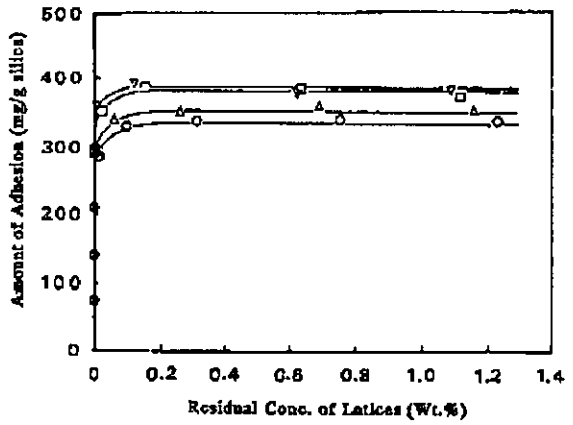

Fig. 11 Adhesion isotherms of amphoteric lattices onto Silica-L at various K_2SO_4 concentrations: (▽) 1.46×10^{-2} M; (□) 1.46×10^{-3} M; (△) 1.46×10^{-4} M; (○) 0 M.

MARCEL DEKKER, INC.
270 Madison Avenue, New York, New York 10016

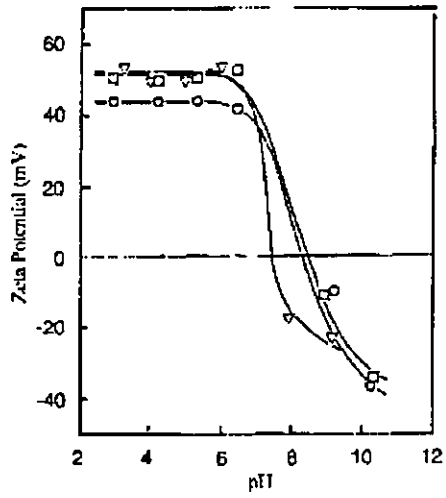

Fig. 12 ζ-Potentials vs. pH curves for heterocoagulate particles prepared at different electrolytes: (∇) heterocoagulates prepared at 2.48×10^{-1} M $MgCl_2$; (O) heterocoagulates prepared at 1×10^{-5} M KCl; (□) amphoteric lattices.

is apparent that the heterocoagulate takes a raspberry shape with one silica particle in the core. In contrast to this, the heterocoagulates generated at a particle size ratio lower than $r=3$ (Fig. 10C and D) are composed of large, irregular aggregates, and regular coagulates were hardly formed at any medium pH and particle number ratio investigated.[31,32]

It is interesting to analyze the different heterocoagulation behaviors from the concept of the adhesion isotherm for the amphoteric lattices on the silica particles. Fig. 11 shows some typical isotherms for the lattices on Silica-L at various K_2SO_4 concentrations, where all the systems were controlled at pH 5.2. It is evident that the isotherms are all well defined and of very high affinity type, and the plateau value increases with increasing K_2SO_4 concentration within the range from 10^{-5} to 10^{-2} mol/dm^3. This means that in this concentration range, adhesion proceeds in a way characteristic of monolayer adhesion. This may be because of the strong blocking effect of adhering particles. However, in K_2SO_4 aqueous solutions more concentrated than 2×10^{-2} mol/dm^3, no reproducible isotherm could be obtained under any conditions tested, and only some irregular aggregates were generated in the course of the experiment.[31] In Fig. 12, the ζ-potentials of the heterocoagulates prepared at different electrolyte concentrations, as well as the data on the amphoteric lattices, are presented as a function of the medium pH. As may be seen, a reversal of charge is observed in all samples, and the IEP in the heterocoagulated systems

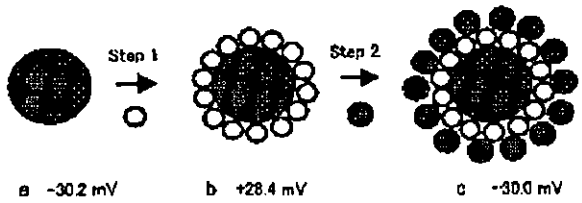

Fig. 13 Schematic showing the process of synthesizing multilayer composite particles: (a) core silica; (b) PC vesicle/silica composite particle; (c) silica/PC vesicle/silica composite particle.

occurs at about pH 8, which is not so different from the IEP of the single lattices. Moreover, the fact that the limiting net positive ζ-potential attained at $3 < pH < 6$ increases with increasing electrolyte concentration is also in line with the increase in latex adhesion with increasing electrolyte concentration.

Multilayer Composite Particles Comprising Silica/Vesicle/Silica Particles

Composite particles, including vesicle particles, are an important topic in application fields. Composite particles can be used frequently in the biomedical field for diagnostic purposes and for treatment medicine. Here, we describe one example of such systems,[33] that is, PC vesicles, which are typical biocolloid systems and are introduced into composites as a one-component particle.

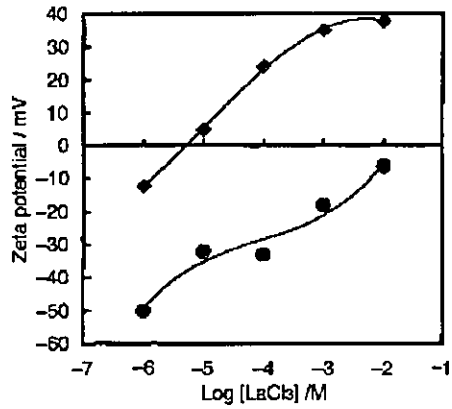

Fig. 14 ζ-Potentials vs. the concentration of $LaCl_3$: (◆) PC vesicles; (●) silica particles.

MARCEL DEKKER, INC.
270 Madison Avenue, New York, New York 10016

The silica/PC vesicle/silica multilayer composite particles were prepared by the alternate adsorption of PC vesicles and small silica particles on the large silica particles with negative charges (Fig. 13). In this study, electrostatic attraction is taken into account as the driving force. It is important that the silica and the vesicle surfaces bear opposite charges to be effective. We can control the surface charges of the vesicle and silica particles by adjusting the concentration of $LaCl_3$. In Fig. 14, the ζ-potentials of PC vesicles and silica particles are shown as a function of $LaCl_3$ concentration. The ζ-potential of PC vesicles decreases with increasing $LaCl_3$ concentration, and becomes positive over a certain concentration of $LaCl_3$. This is because of the binding effect of La^{3+} ions to the phospholipids head group.[34] However, for silica dispersions, the ζ-potential remained negative over the 10^{-6}–10^{-2} M concentration range of $LaCl_3$. Thus at 10^{-4} M $LaCl_3$, the ζ-potentials of the silica and PC vesicles were -30 and $+32$ mV, respectively. It is assumed that a strong electrostatic attraction will occur between the vesicles and the silica particles. Therefore we selected 10^{-4} M $LaCl_3$ as the heterocoagulation condition.

After mixing the PC vesicles with the core silica dispersion, the free vesicles were removed from the dispersion and the ζ-potentials of the composite particles generated were measured. The value was determined to be +28 mV. The positive ζ-potential indicates that the PC vesicles are adsorbed on the silica surface because the surface of the PC vesicles binds with La^{3+} ions.

For the PC vesicle adsorption state on the silica surface, there are two possible states: 1) as a vesicle particle layer, or 2) as a lipid molecular bilayer. To clarify the adsorption state of the vesicles, as the next stage, the adsorption amounts of PC on the silica surface have been measured. In Fig. 15, the results are shown as a function of the PC concentration. Adsorption amounts are expressed by the number of phospholipids molecules ad-

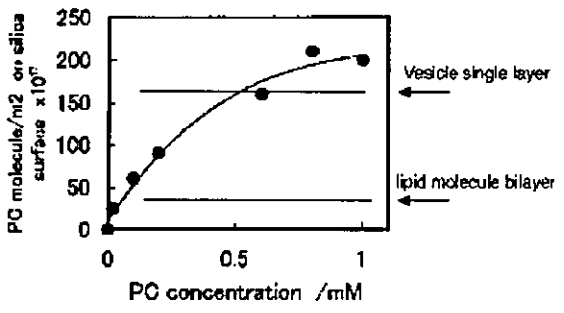

Fig. 15 Adsorption amount for PC on core silica surface in 10^{-4} M $LaCl_3$ at 25°C.

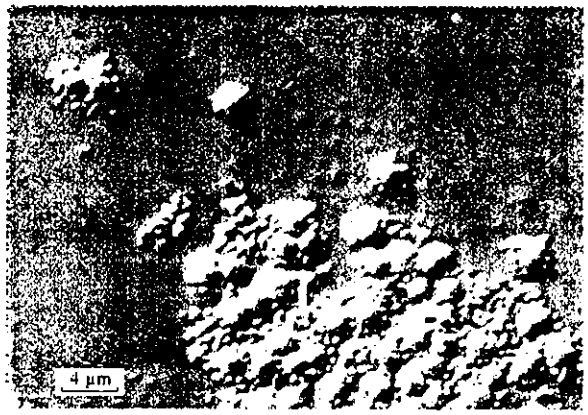

Fig. 16 Optical micrograph of silica/PC vesicles/silica composite particles. (*View this art in color at www.dekker.com.*)

sorbed per square meter of silica surface. The solid line represents a theoretical curve for the adsorption amount of the single bilayer model, assuming the area per PC molecule equals 0.7 nm^2. The dotted line shows a theoretical curve for the adsorption of a single vesicle layer model, assuming that the vesicles are of uniform size and have a unilamellar spherical shape. The saturated adsorption amounts in the experiments are located near the value for the latter, but over it. This is because of the existence of some multilamellar PC vesicles in the sample (i.e., the existence of multilamellar PC vesicles will induce a large number of PC molecules than the value of unilamellar vesicles). Thus we can expect that the PC vesicles will be adsorbed on the silica surface as a unilamellar vesicle layer (i.e., the composite particles have been generated as shown in Fig. 13b). Furthermore, we then separated the PC vesicle/silica composites from the free PC vesicles by the ultra-filtration method (with a polycarbonate membrane filter, pore size 1.0 μm), and determined the mean size of the composite particles by the dynamic light scattering (DLS) method. The diameter of the composite particles is 1.93 μm, and this value is close to 1.9 μm, which was calculated by the single particle layer model. This result means that the PV vesicles will be adsorbed on silica particles as the same spherical particle size.

In the second stage of composite formation, we mixed the PC vesicle/silica composite particles with a small silica ($2a$=0.5 μm) dispersion under the same 10^{-4} M $LaCl_3$ solution. The ζ-potentials of the products reversed from positive (+28.4 mV) to negative (-30 mV) again, which indicates that the small silica particles (with negative charges) were adsorbed on the surface of the positively charged composite particles (Fig. 13c).

MARCEL DEKKER, INC.
270 Madison Avenue, New York, New York 10016

The direct observation of the multilayer formation of composite particles is provided by a special optical microscopy technique. In Fig. 16, the composite particles of the silica/PC vesicle/core silica in the 10^{-4} M $LaCl_3$ solution are shown. We cannot clearly see the image of the PC vesicles on the silica because the PC vesicle has a large water core and a thin lipid bilayer (about 5 nm). Therefore the total refractive indices of the PC vesicle are close to those of water. However, the formation of the silica/PC vesicle/silica composite particles is indicated clearly in Fig. 16; the small silica particles are adsorbed on the spherical surface of the PC vesicle/core silica composite and are located on the outer layer of the composite particles.

The Buildup of Polyelectrolyte and/or Colloid Particle Multilayer on Solid Surfaces

The multilayer formation of polyelectrolytes on colloid particles is usually characterized by a stepwise increase of the adsorbed amount and layer thickness, and by alternating highly positive and negative ζ-potentials of the covered particles. Here, we describe two kinds of multicomponent layer systems using polyelectrolyte and colloid particles. One is the formation of polyelectrolyte multilayers on polymer colloids. Another is the formation of composite particles including organic and inorganic colloid particles using a layer-by-layer technique of polyelectrolytes.[35]

To emphasize the influence of the polarity of the substrate, three kinds of polystyrene lattices are employed. PS-740 lattices with large size ($2a$=740 nm) were prepared by the usual surfactant-free emulsion polymerization technique;[12] NaSS-190 lattices were made by incorporating a small amount of an ionic comonomer, sodium-*p*-vinylbenzyl-sulfate, into the polystyrene chain according to Kotera et al.[13] The charge density of NaSS-190 lattices is much higher than that of PS-740 latex. DEAM-250 lattices consist of amphoteric particles prepared by the method described by Homola and James.[36] Characteristic data for these samples are shown in Table 3. Silica samples with different particle sizes ($2a$=500, 300, and 20 nm), which were obtained from Nippon Catalisitic Co. Ltd. and Nissan Chemical Co. Ltd., were used. All these single dispersions consisted of monodisperse spherical particles with $D_w/D_n < 1.04$ always, and were used after extensive dialysis.

As the cationic polymer, poly-L-lysine (PLL-19) with a fixed molecular weight (M=190,000) was used, and as the anionic polymer, polystyrene sulfonate (PSSNa-50) with M=500,000 was used. PSSNa-50 carries a constant charge for pH 3–10. However, PLL-19 is pH-dependently charged and it is known that a fixed positive charge is carried only in the region of pH 3–7.

The adsorption of polyelectrolytes was allowed to take place for 1.5–2 hr at a 0.1–0.3 mg/mL PLL or PSSNa solution using a very dilute latex or silica suspension (ϕ=0.0001) and a saturated concentration without any free polymer of each polyelectrolyte that was determined by mobility measurements of the core particles. During the adsorption process, suspensions of the core particles were mixed slowly by means of rotating end-over-end.

The DLS measurements were carried out to assess the development of hydrodynamic layer thickness on the addition of PLL or PSSNa molecules. The heterocoagulated state of composite particles was observed directly by the optical microscope and scanning electron microscope.

Multilayer formation of polyelectrolytes on colloid particles

In Fig. 17, a typical cyclical curve of ζ-potential on alternating additions of PLL-19 and PSSNa-50 on negatively charged NaSS-190 latex surfaces is shown. The switch to either of the new polyelectrolytes is

Table 3 Particle diameters, ζ-potentials, and functional groups of the colloids

Particle	Diameter (nm)	ζ-Potential (mV) in 10^{-3} M NaCl	Functional group
NaSS-190 latex	190	− 50 (pH 4)	SO_3^-
DEAM-250 latex	252	+ 60 (pH 4)	$)NH^+$
PS-740 latex	740	− 30 (pH 4)	OSO_3^-
Silica-500	500	− 30 (pH 6)	SiO_2^-
Silica-300	300	− 30 (pH 6)	SiO_2^-
Silica-20	20	− 30 (pH 6)	SiO_2^-

MARCEL DEKKER, INC
270 Madison Avenue, New York, New York 10016

indicated by the arrows. In the figure, the abscissa axis indicates the total number of repeating units of both polyelectrolyte molecules. The change of the ζ-potential is substantial (i.e., the ζ-potential is highly positive after the addition of PLL-19 and highly negative after the addition of PSSNa-50). This result indicates clearly that, on the adsorption of polyelectrolyte, the oppositely charged surface is not just compensated but strongly overcompensated. An overcompensation of polyelectrolyte adsorption is the main reason for progressing the multilayer formation. The buildup process was also confirmed from the stepwise increase of the layer thickness of the core latex particles. The stepwise increase of the layer thickness, especially after the adsorption of PSSNa-50 molecules on the core particle surfaces, is also shown in Fig. 17.

In the next stage, we tried to produce polyelectrolyte multilayers under different medium compositions. In Fig. 18, the results of multilayer formations of PSSNa-50 and PLL-19 in pure water at pH 4, 10^{-2} M NaCl solution, and 10^{-2} M $BaCl_2$ solution are indicated. In these experiments, the positively charged DEAM-250 lattices were used as the core particles. In this figure, the

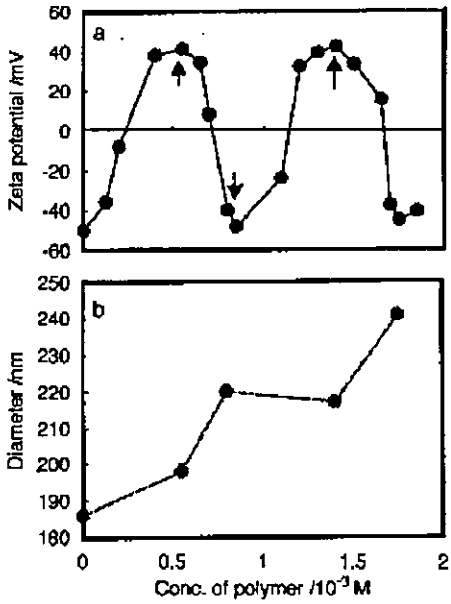

Fig. 17 ζ-Potential (a) and total particle size (b) of the composite system by multilayer deposition of PLL-19 and PSSNa-50 on NaSS-10 lattices against the concentrations of each polyelectrolyte solution ($\phi = 7.5 \times 10^{-3}$ wt.%, pH 4, [NaCl] = 1×10^{-3} M). The switch to a new polymer solution is indicated by the arrows.

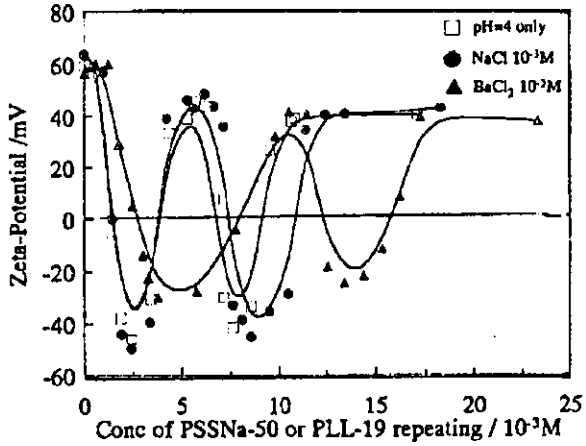

Fig. 18 ζ-Potential of multilayers of PSSNa-50 and PLL-19 on DEAM-250 lattices against the concentrations of each polyelectrolyte solution under different salt conditions ($\phi = 7.5 \times 10^{-3}$ wt.%, pH 4).

locus of ζ-potentials obtained under different salt conditions is plotted for the total amounts of repeating units of PLL-19 and PSSNa-50 molecules. As can be seen, the step in the ζ-potential obtained in the $BaCl_2$ solution is delayed, indicating that the electrostatic attraction between PSSNa-50 and the charged surface of DEAM-250 lattices is weakened. This is caused by the strong affinity of Ba^{2+} to SO_3^- in PSSNa-50 molecules. The existence of such a specific effect has been reported in the literature.[37,38]

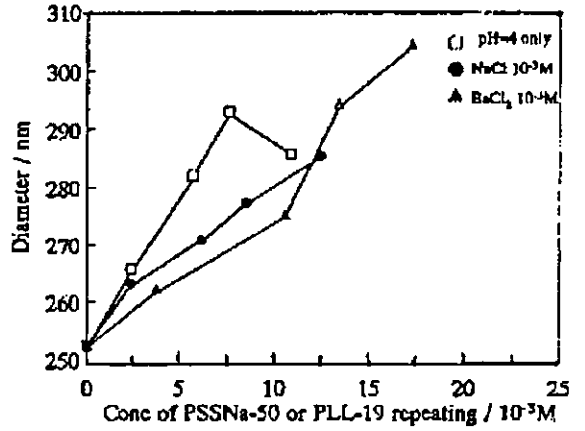

Fig. 19 The total particle sizes in each step to stable multilayers of PSSNa-50 and PLL-19 on DEAM-250 lattices under different salt conditions ($\phi = 7.5 \times 10^{-3}$ wt.%, pH 4).

MARCEL DEKKER, INC.
270 Madison Avenue, New York, New York 10016

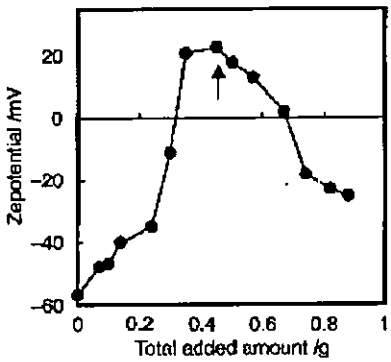

Fig. 20 ζ-Potential of composite particles by multilayer deposition of PLL-19 (concentration, 2×10^{-4} wt.%) and Silica-300 (concentration, 1.0×10^{-3} wt.%) on PS-740 lattices ($=7.5 \times 10^{-4}$ wt.%, pH 6, [NaCl]$=1 \times 10^{-3}$ M). The switch to Silica-300 from PLL-19 is indicated by the arrow.

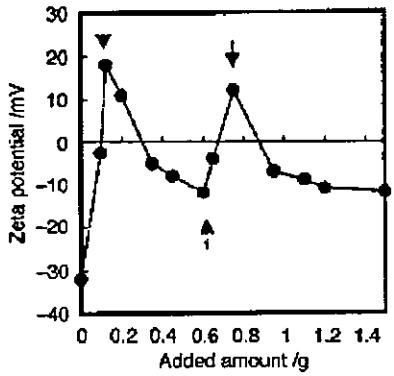

Fig. 22 ζ-Potential of composite particles by multilayer deposition of pair (PLL-19 + Silica-20) layers. The switch is indicated by the arrow.

Fig. 19 indicates the stepwise increase of layer thickness on DEAM-250 latex particles under different salt conditions. Surprisingly, in the 10^{-2} M $BaCl_2$ solutions, the layer thickness of adsorbed polyelectrolytes increased steadily and the weak attraction effect coming from Ba^{2+} was not observed on the layer-by-layer formation. However, in distilled water, the layer thickness increased quickly at an early stage of deposition. However, in the final stage, the layer shrunk. The reason for this phenomenon cannot be explained, but this result indicates surely that strong electrostatic attraction is not always the sole factor necessary to form a stable multilayer.

Multilayer formation of colloid particles with polyelectrolytes

The layer-by-layer deposition technique of polyelectrolytes can be applied to the formation of composite particles comprising organic and inorganic colloid particles.

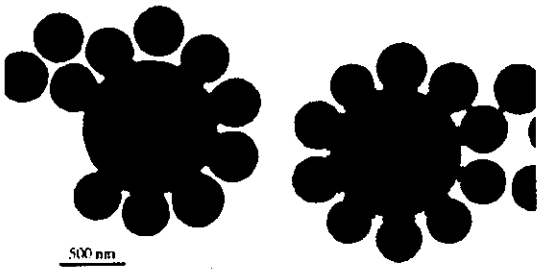

Fig. 21 Electron micrograph showing hybrid particles of outer Silica-300 particles on core PS-740 lattices.

Fig. 20 shows the buildup processes of colloid particles using PS-740 latex sample as the core. Here, PLL-19 was used as a binder polyelectrolyte. The abscissa axis in this figures indicates the total amounts of the binder polyelectrolyte + adhering particles. As can be seen from the figure, the ζ-potential of the core particle has changed from a negative value to a positive value by adsorption of PLL-19 molecules, and changed again to negative values with an increasing number of adhering silica particles (Silica-300). These results suggest that the composite formation of colloid particles has progressed reasonably by the binder layer of PLL-19 molecules. Fig. 21 is a photograph showing a typical example of hybrid particles consisting of outer Silica-300 particles on core PS-740 latex as prepared in this experiment. It is known that the composite consists of regular hybrid particles comprising organic and inorganic particles. However, the structure form is not so stable and sometimes the system includes free silica particles.

In the next stage, the synthetic process of hybrid particles with multilayers of silica particles on PS-740 was examined. As the binder polyelectrolyte, the PLL-19 molecule was also used under the same medium conditions. Fig. 22 shows the cyclical behavior of the ζ-potential in the formation process of multilayers of Silica-20 and PLL-19 layers. As can be seen, the cycle of ζ-potential after adhesion is systematical, indicating that the deposition of PLL and Silica-20 has progressed regularly. Fig. 23 is a photograph of an original PS-740 latex and two kinds of composite particles covered with a single silica + polymer layer and two silica + polymer layers. Two kinds of composite particles can be distinguished based on the thickness of the adhering silica particle layer.

MARCEL DEKKER, INC.
270 Madison Avenue, New York, New York 10016

Fig. 23 Electron micrograph showing hybrid particles of small Silica-20 particles on core PS-740 latex particles: (a) PS-740 lattices; (b) hybrid particles deposited by a single (PLL-19 + Silica-20) layer; (c) hybrid particles deposited by pair (PLL-19 + Silica-20) layers.

From these results, it is concluded that, by combining a multilayer formation of polyelectrolytes and charged colloid particles, we can prepare many new synthetic materials comprising different chemical species, different structures, and different shapes.

CONCLUSION

Here, several preparation processes of composite particles relating to the electrical properties of particles are described: 1) the heterocoagulation process of amphoteric polymer lattices on spherical silica; 2) composite formation comprising silica/vesicle or silica/vesicle/silica particles; and 3) the buildup process of polyelectrolyte or colloid particle multilayers on latex or silica surfaces. All these results indicate that the electrokinetic measurement is an essential and powerful technique for monitoring the formation process of composite particles with different compositions. Finally, the present authors would like to stress that the formation processes described here were concerned with the semimicron-sized particles, but these techniques can be applied to systems, including nanosized particles with slight reversions.

REFERENCES

1. Matijevic, E. *Interfacial Electrokinetics and Electrophoresis*; Delgado, A.V., Ed.; Surfactant Science Series, Marcel Dekker, Inc.: New York, 2002; Vol. 106, 199–218.
2. *Electrical Phenomena at Interfaces*; Ohshima, H., Furusawa, K., Eds.; Surfactant Science Series, Marcel Dekker, Inc.: New York, 1998; Vol. 76.
3. Lyklema, J. *Fundamentals of Interface and Colloid Science*; Academic Press, Inc.: London, 1995; Vol. II.
4. von Smoluchowski, M. *Handbuch der Electrizitat und des Magnetismus*; Graetz, W., Ed.; Barth: Leipzig, 1914; Vol. II, 366.
5. Komagata, S. Nihon Kagaku Kaishi **1932**, *53*, pp. 342, 969.
6. Furusawa, K.; Uchiyama, K. J. Colloid Interface Sci. **1998**, *140*, 217.
7. Sasaki, H.; Muramatsu, A.; Arakatsu, H.; Usui, S. J. Colloid Interface Sci. **1991**, *142*, 266.
8. Usui, S.; Imamura, Y.; Sasaki, H. J. Colloid Interface Sci. **1987**, *118*, 335.
9. Marlow, B.J.; Fairhurst, D.; Pendse, H.P. Langmuir **1988**, *4*, 611.
10. O'Brien, R.W.; Midmore, B.R.; Lamb, A.; Hunter, R.J. Faraday Discuss. Chem. Soc. (London) **1990**, *90*, 301.
11. Dukhin, A.S.; Shilov, V.N.; Oshima, H.; Goetz, P.J. Langmuir **1999**, *15*, pp. 6692, 3445.
12. Hozumi, Y.; Furusawa, K. Colloid Polym. Sci. **1990**, *268*, 469.
13. Kotera, A.; Furusawa, K.; Takeda, Y. Kolloid-Z. Z. Polym. **1970**, *239*, 677.
14. Juang, M.S.; Krieger, I.M. J. Polym. Sci. **1976**, *14*, 2089.
15. Van den Hul, H.J.; Vanderhoff, J.W. Electroanal. Chem. **1972**, *37*, 161.
16. Kolthoff, I.M.; Miller, I.K. J. Am. Chem. Soc. **1951**, *73*, 3055.
17. Ottewill, R.H.; Shaw, J.N. Kolloid-Z. Z. Polym. **1976**, *218*, 34.
18. Hearn, J.; Ottewill, R.H.; Shaw, J.N. Br. Polym. J. **1972**, *2*, 116.
19. Levine, S.; Neale, G.; Epstein, N. J. Colloid Interface Sci. **1976**, *57*, 427.
20. Greenwood, R.; Bergstrom, L. J. Eur. Ceram. Soc. **1997**, *17*, 537.
21. Furusawa, K.; Anzai, C. Colloid Polym. Sci. **1987**, *265*, 882.

MARCEL DEKKER, INC.
270 Madison Avenue, New York, New York 10016

22. Furusawa, K.; Kimura, Y.; Tagawa, T. J. Colloid Interface Sci. **1986**, *109*, 69.
23. Velev, O.D.; Furusawa, K.; Nagayama, K. Langmuir **1996**, *12*, pp. 2374, 2385.
24. Wilcox, D.L.; Berg, M. Hollow and Solid Spheres and Microspheres. In *Proceedings of the Materials Research Society, Pittsburgh*; Wilcox, P.L., et al., Eds.; Science and Technology Associated with Their Fabrication and Application, 1995; Vol. 372, 3–13.
25. Iier, K.K. J. Colloid Interface Sci. **1966**, *21*, 569.
26. Decher, G.; Hong, J.D. Ber. Bunsenges. Phys. Chem. **1991**, *95*, 1439.
27. Decher, G. Science **1997**, *277*, 1232.
28. Caruso, F.; Mohwald, H. Langmuir **1999**, *8276*, 15.
29. Caruso, F.; Caruso, R.A.; Mohwald, H. Science **1988**, *1111*, 282.
30. Gherardi, P.; Matijevic, E. Colloid Interface Sci. **1986**, *109*, 57.
31. Furusawa, K.; Anzai, C. Colloids Surf. **1992**, *63*, 103.
32. Furusawa, K.; Velev, O.D. Colloids Surf., A Physicochem. Eng. Asp. **1999**, *159*, 359.
33. Yang, B.; Matsumura, H.; Katoh, K.; Kise, H.; Furusawa, K. Langmuir **2001**, *17*, 2283.
34. Lehrmann, R.; Seeling, J. Biochim. Biophys. Acta **1994**, *1189*, 89.
35. Furusawa, K.; Satou, S. Colloids Surf. **2001**, *195*, 143.
36. Homola, A.; James, R.M. J. Colloid Interface Sci. **1977**, *59*, 123.
37. van Duelm, P.; Norde, W.; Lyklema, J. J. Colloid Interface Sci. **1977**, *59*, 123.
38. Furusawa, K.; Tomotsu, N. J. Colloid Interface Sci. **1983**, *93*, 504.

MARCEL DEKKER, INC.
270 Madison Avenue, New York, New York 10016

P1-273 Glutamate responses of the retinal neurons recording with voltage sensitive dye

Yukio Shimoda[1]
[1]Medical Research Institute, Tokyo Women's Medical University,Tokyo, Japan

The photo information processing in vertebrates retina starts from the release of the glutamate from the photoreceptor cells. Therefore, it can know the mechanism of information processing in the retina by recording the response to extringic application of the glutamate. After making transverse sections of the dace retina, they were stained with voltage sensitive dye (Nihon Kanko Shikiso, NK-2761) and they were put on the microscope stage. A small amount of monosodium glutamate was applied through the glass micro pipette to the each layer of the retina. The responses were recorded as the optical density changes depending on membrane potential. The depolarization was recorded in the horizontal cells when the glutamate was applied to the outer plexiform layer. The depolarization was observed in the inner nuclear and plexiform layer. In some cells in the inner nuclear layer, hyoperpolarizing responses were recorded. It is thought that the mechanism of the photo information processing can be clarified by detailed identification of the cells.

Available online at www.sciencedirect.com
SCIENCE DIRECT
Virus Research 108 (2005) 23–28
Virus Research
www.elsevier.com/locate/virusres

A lentiviral expression system demonstrates that L* protein of Theiler's murine encephalomyelitis virus (TMEV) is essential for virus growth in a murine macrophage-like cell line

Toshiki Himeda[a], Yoshiro Ohara[a,*], Kunihiko Asakura[a], Yasuhide Kontani[a], Manabu Murakami[b], Hiromi Suzuki[c], Makoto Sawada[c]

[a] *Department of Microbiology, Kanazawa Medical University, 1-1 Uchinada, Ishikawa 920 0293, Japan*
[b] *Division of Basic Science, Medical Research Institute, Kanazawa Medical University, 1-1 Uchinada, Ishikawa 920 0293, Japan*
[c] *Institute for Comprehensive Medical Science, Fujita Health University, Aichi 470 1192, Japan*

Received 14 April 2004; received in revised form 14 July 2004; accepted 19 July 2004
Available online 17 September 2004

Abstract

The DA subgroup strains of Theiler's murine encephalomyelitis virus (TMEV) synthesize L* protein, which is translated out of frame with the polyprotein from an alternative AUG, 13 nucleotides downstream from the authentic polyprotein AUG. By a 'loss of function' experiment using a mutant virus, DAL*-1, in which the L* AUG is mutated to an ACG, L* protein is shown to play an important role in virus persistence, TMEV-induced demyelination, and virus growth in macrophages. In the present study, we established an L* protein-expressed macrophage-like cell line and confirmed the importance of L* protein in virus growth in this cell line.

Keywords: Theiler's murine encephalomyelitis virus; L* protein; Lentiviral vector; Virus growth; Macrophages

Theiler's murine encephalomyelitis virus (TMEV) belongs to the genus *Cardiovirus* of the family *Picornaviridae* and is divided into two subgroups (Ohara and Roos, 1987; Lipton and Jelachich, 1997; Obuchi and Ohara, 1998; Roos, 2002). DA (or TO) subgroup strains induce a non-fatal polioencephalomyelitis in weanling mice followed by virus persistence and chronic demyelination in the spinal cords. This late demyelinating disease serves as an experimental model of the human demyelinating disease, multiple sclerosis. In contrast, GDVII subgroup strains cause acute fatal polioencephalomyelitis without demyelination. The precise mechanisms of virus persistence and demyelination caused by DA subgroup strains are still unknown. A 17 kDa protein, called L*, is translated out of frame with the polyprotein from an alternative AUG, 13 nucleotides downstream from the authentic polyprotein AUG (Kong and Roos, 1991; Obuchi and Ohara, 1998; Roos, 2002). L* protein is only synthesized in the DA subgroup strains since the L* AUG is present in DA subgroup strains, but not in GDVII subgroup strains (Michiels et al., 1995; Obuchi and Ohara, 1998; Roos, 2002). Therefore, L* protein is thought to be a key protein regulating DA biological activities. A 'loss-of-function' experiment using a mutant virus, DAL*-1, in which the L* AUG initiation codon is mutated to an ACG, demonstrated that L* protein plays an important role in DA persistence and demyelination (Chen et al., 1995; Ghadge et al., 1998). However, that finding is still controversial since the absence of the L* AUG initiation codon in a different DA infectious clone had only a weak influence on the persistence of DA strain (van Eyll and Michiels, 2000, 2002).

We previously reported that DA strain grows in J774-1 cells, an *H-2*^{d} macrophage-like cell line derived from a tumor of a BALB/c mouse (Ralph et al., 1975), while the GDVII

* Corresponding author. Tel.: +81 76 218 8096; fax: +81 76 286 3961.
E-mail address: ohara@kanazawa-med.ac.jp (Y. Ohara).

0168-1702/$ – see front matter © 2004 Elsevier B.V. All rights reserved.
doi:10.1016/j.virusres.2004.07.009

strain does not (Obuchi et al., 1997). This phenomenon is of great interest since a major site for TMEV persistence is thought to be macrophages (Lipton and Jelachich, 1997; Obuchi and Ohara, 1998; Roos, 2002). The important role of L* protein in this in vitro phenomenon can be demonstrated by using DAL*-1 virus. DAL*-1 virus does not grow in murine monocyte/macrophage lineage cell lines, but it does grow in other cell lines, including neural cells (Obuchi et al., 1999). A recombinant virus, DANCL*/GD, which has the DA 5′ noncoding and L* protein coding regions replacing the corresponding regions of GDVII and therefore synthesizes L* protein, had a rescue of growth activity in J774-1 cells, suggesting that L* protein plays an important role in virus growth in macrophages (Obuchi et al., 2000).

A challenge in research related to L* protein is that its sequence overlaps with that of the polyprotein, making it impossible to introduce the DA L* coding sequence into the parental GDVII strain without changing the polyprotein sequence. The generation of macrophage cells that constitutively express L* protein would allow a confirmation of the role of this protein in virus growth with a 'gain of function' experiment. This system would also allow the synthesis of L* protein in the cytoplasm, as has been described (Obuchi et al., 2001), without being incorporated into virions. Therefore, the goal of the present study was to establish a macrophage cell line that constitutively expresses L* protein.

We used a lentiviral expression system in order to achieve a stable and efficient gene transfer of L* protein. The vector was constructed by using the transfer vector plasmid pCSII-EF-MCS-IRES-hrGFP, constructed by Dr. Hiroyuki Miyoshi and Dr. Tomoyuki Yamaguchi, Laboratory of Genetics, The Salk Institute for Biological Studies. The plasmid has sequences of a human elongation factor (EF) 1 α subunit gene promoter, a multiple cloning site (MCS), an internal ribosome entry site (IRES), and the coding region of a 'humanized, red-shifted' green fluorescent protein (hrGFP) in tandem. L* coding sequence was inserted into MCS, resulting in the production of L* protein independently from hrGFP and not as a fusion protein. The expression of both proteins is regulated by one promoter. Another construct, in which the 3xFLAG epitope sequence is tagged to the N-terminus of L* protein, was generated as an additional control since the 5′ one third of the L* protein coding region is important for its function (Obuchi et al., 2001). In order to generate vesicular stomatitis virus (VSV) G protein-pseudotyped lentiviral vector particles, the transfer vector plasmid pCSII-EF-(cDNA of L* or 3xFLAGL* protein)-IRES-hrGFP with the packaging plasmid pMDLg/pRRE, pRSV-Rev, and the VSV-G protein envelope plasmid pMD.G (Naldini et al., 1996) were tansfected into subconfluent 293T cells, a human embryonic kidney epithelial cell line expressing the simian virus 40 large T antigen, using a high-efficiency calcium-phosphate-mediated transfection method (Miyoshi et al., 1997; Miyoshi et al., 1998; Sambrook and Russell, 2001). High-titer virus stocks were prepared by centrifugation (43,600 × *g*, 3 h, 21 °C). The infectious titers were determined by counting the number of GFP-positive cells by fluorescence-activated cell sorting (FACS) analysis (FACSCalibur: BD Biosciences, San Jose, CA). J774-1 cells (2×10^5) were infected and transduced at a multiplicity of infection (M.O.I.) of 5. After the infection, the third subculture of L*-transduced and 3xFLAGL*-transduced J774-1 cells were seeded at a density of 0.5 cells per well onto 360 wells and 1200 wells of HLA plates (Greiner bio-one, Tokyo, Japan), respectively.

Cell propagation was observed in 27 wells of L*-transduced cells and 105 wells of 3xFLAGL*-transduced cells. During the first several passages, the cells in approximately 50% of wells were GFP-positive and propagated more slowly than the original J774-1 cells. Some showed a different morphology, such as enlargement (20–30 μm, about 1.5-fold larger in diameter) and an amoebic shape. We selected four L*-expressed (L*/J774) and eight 3xFLAGL*-expressed (3xFLAGL*/J774) clones by FACS analysis using expression of GFP. The cells formed clusters easily when replated in new culture dishes. These properties reverted to those of the original J774-1 cells after seven passages. When both cells were seeded in a 35 mm plastic culture dish at the density of 1×10^5 cells/ml, the cultures reached to the density of 1×10^6 cells/ml within about four days, with a doubling time of 24–30 h. Seven empty vector-transduced clones (control/J774) were also obtained from the empty vector-transduced J774-1 cells and served as a control. The properties of these cells were not different from those of the original J774-1 cells. Fig. 1 shows the histograms of L*/J774/6, 3xFLAGL*/J774/33 and control/J774/6 clones, which gave the highest GFP expression.

The expression of L* and 3xFLAGL* proteins was further confirmed by Western blotting using polyclonal rabbit anti-L* antibody (Ab) (Obuchi et al., 2000, 2001) or monoclonal mouse anti-FLAG M2 Ab (Sigma, St. Louis, MO). Enhanced chemiluminescence reagents, ECL plus (Amersham Biosciences, Buckinghamshire, UK), detected biotinylated secondary Ab and horseradish peroxidase-conjugated streptavidin (Fig. 2). The expression of L* or 3xFLAGL* protein was stable after forty passages of culture.

We examined and compared the growth kinetics of DAL*-1 virus in those cells. The culture supernatants and cell lysates of 1.5×10^6 cells infected with DAL*-1 virus at an M.O.I. of 10 PFU per cell were harvested at 0, 3, 6, 12, 24, and 48 h post-infection (p.i.), and the infectivity was assayed by a standard plaque assay on BHK-21 cells. In L*/J774/6 cells, the titers of cell-free and cell-associated DAL*-1 virus reached a peak at 12 h p.i. (6.3×10^5 and 3.8×10^5 PFU/ml, respectively) and then gradually decreased (Fig. 3B). On the other hand, the titers gradually decreased in control/J774/6 cells (Fig. 3A). The data indicated that L* protein is essential for DA growth in J774-1 cells. The titers of DAL*-1 virus also gradually decreased in 3xFLAGL*/J774/33 cells (Fig. 3C), suggesting that the N-terminus is important for the function of L* protein, as previously reported (Obuchi et al., 2001). In addition, even though the 3xFLAG epitope is a small peptide (2.7 kDa), it may have changed the higher-order structure of

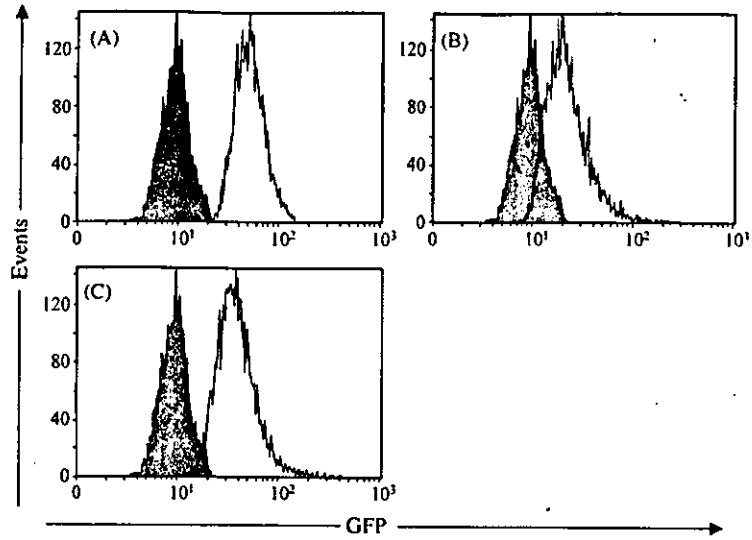

Fig. 1. Flow cytometric analysis of green fluorescent protein (GFP) fluorescence. J774-1 cells were infected and transduced with lentiviral vector containing the L* or 3xFLAGL* protein sequence. The transduced cells were cloned by a limiting dilution. Figure shows the histograms of GFP fluorescence in the representative clone of the vector-transduced J774-1 cells (open area). The original J774-1 cells served as a control (closed area). (A) Control/J774/6, which was transduced by an empty vector as described in the text; (B) L*/J774/6, which was transduced by the vector containing the L* sequence; (C) 3xFLAGL*/J774/33, which was transduced by the vector containing the 3xFLAGL* sequence.

L* protein since L* protein is relatively small (17 kDa). Also, the predicted hydrophilicity of 3xFLAG epitope may have interfered with the strong hydrophobicity of L* protein (Ohara et al., 1988; Obuchi et al., 2001), and thereby disturbed the function of L* protein.

To further investigate which step of virion formation is affected by L* protein, viral RNA synthesis of DAL*-1 virus following the infection of those cells was analyzed by RNase protection assay (RPA) (Fig. 4A). RPA was performed with the BD RiboQuant™ Non-Radioactive RPA system (BD Biosciences, San Jose, CA), according to the manufacturer's instructions. Briefly, pDAFL3, a full-length infectious DA cDNA clone (Roos et al., 1989), was cleaved at the *Hinc*II site (nt 7783) in the viral genome in order to prepare an antisense probe. The linearized plasmid was transcribed by an in vitro transcription system with T3 RNA polymerase in the presence of biotin-16-UTP (Roche Diagnostics GmbH, Mannheim, Germany). The biotin-labeled RNA probe con-

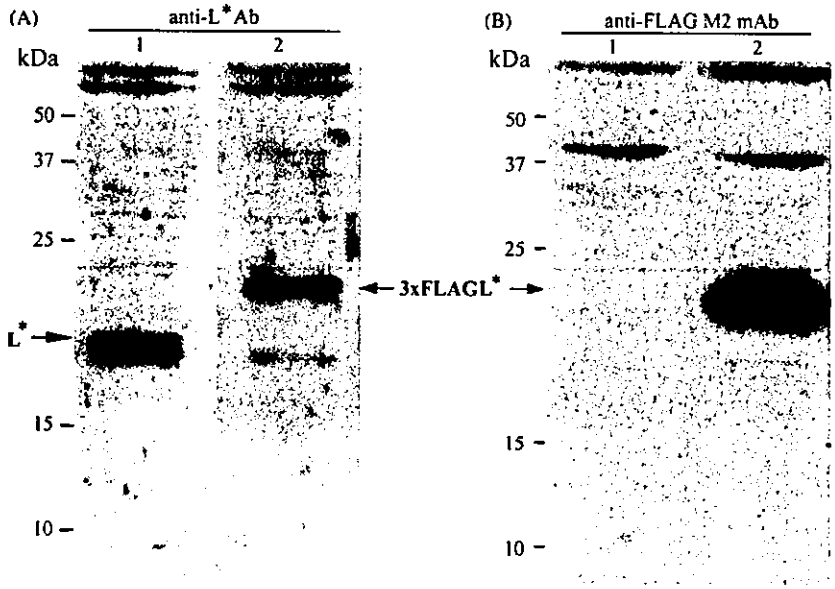

Fig. 2. Protein expression of the transgenes (L* and 3xFLAGL* sequences) in L*/J774/6 and 3xFLAGL*/J774/33 cells. The expression of L* gene in L*/J774/6 cells or 3xFLAGL* gene in 3xFLAGL*/J774/33 cells was analyzed by Western blotting as described in the text. L* (lane 1) and 3xFLAGL* (lane 2) proteins were detected with anti-L* antibody (A) and anti-FLAG M2 monoclonal antibody (B), respectively.

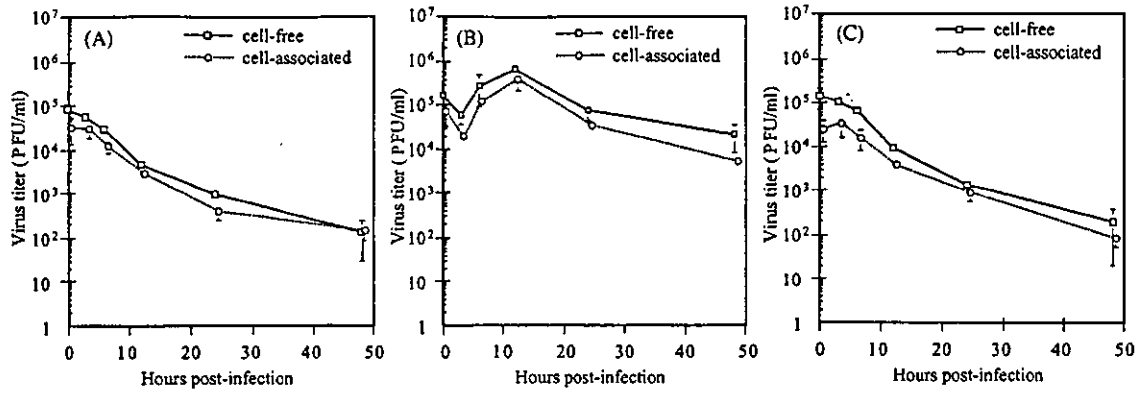

Fig. 3. Growth kinetics of DAL*-1 virus in control/J774/6 (A), L*/J774/6 (B), and 3xFLAGL*/J774/33 (C) cells. The culture supernatants (solid lines, open squares) and cell lysates (broken lines, open circles) of cells infected at a multiplicity of infection (M.O.I.) of 10 were harvested at indicated time points and subjected to titer determination by a standard plaque assay on BHK-21 cells. Data are expressed as the mean ± standard deviation (S.D.) in three independent experiments.

tained 310 nt of sequence complementary to the 3' region of the viral genome and 52 nt of vector sequence (Ohara et al., 1988; Roos et al., 1989). At 0, 3, 6, and 9 h p.i., total RNA was extracted and purified from 9.3×10^4 virus-infected cells by using RNeasy Mini Kit (QIAGEN, Tokyo, Japan). The RNA and 10 ng of biotin-labeled RNA probe were hybridized, and then treated with RNase A and RNase T1. The protected RNA probes were separated by electrophoresis on 5% polyacrylamide gels containing 8 M urea, and transferred to positively-charged nylon membranes by electroblotting. The signals were detected by chemiluminescent detection system. As shown in Fig. 4A, the amount of viral RNA of DAL*-1 virus clearly increased and reached a peak 6 h p.i. in all the cells examined.

Viral protein synthesis was also examined in those cells. At 3, 6, and 9 h p.i., 1×10^6 cells infected with DAL*-1 virus were scraped and dissolved in sample buffer (0.01 M Tris-Cl [pH 6.8], 1 mM EDTA, 2.5% SDS, 5% 2-mercaptoethanol, 10% glycerol, 0.005% bromophenol blue). The cell lysates were analyzed by Western blotting with DA-neutralizing monoclonal antibody, DA mAb 2, which reacts to VP1 capsid protein of DA strain (kindly provided from Dr. Raymond P. Roos, University of Chicago, IL) (Fig. 4B). The amount of VP1 capsid protein of DAL*-1 virus increased rapidly from

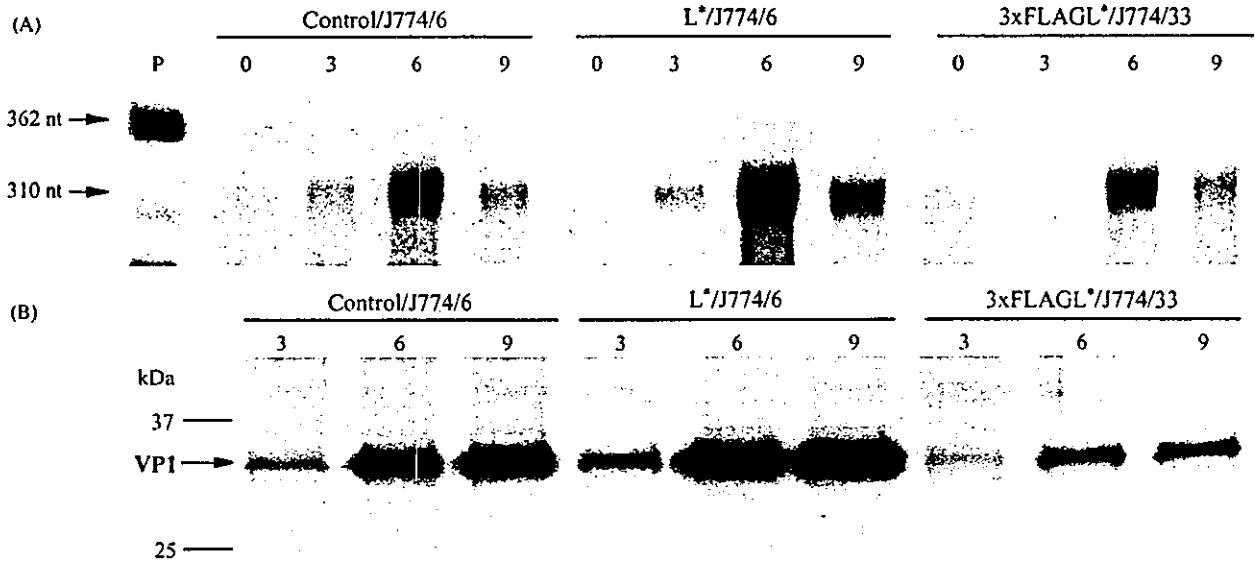

Fig. 4. (A) Viral RNA synthesis of DAL*-1 virus in control/J774/6, L*/J774/6, and 3xFLAGL*/J774/33 cells. Total RNA extracted from the virus infected-cells (9.3×10^4 cells) was subjected to RNase protection assay as described in the text. The numbers at the top of panel indicate hours post-infection (p.i.). Lane P is the starting probe. (B) Synthesis of viral protein in control/J774/6, L*/J774/6, and 3xFLAGL*/J774/33 cells. The cells were infected with DAL*-1 virus at an M.O.I. of 10. After the infection, the cell lysates were analyzed by Western blotting with DA mAb 2 as described in the text. The numbers at the top of panel indicate hours p.i.

3 h p.i., reaching a plateau at 6 to 9 h p.i. in L*/J774/6 cells. The same tendency was observed in both control/J774/6 and 3xFLAGL*/J774/33 cells.

The data obtained in the L*-expressed system have confirmed that L* protein is essential for virus growth in J774-1 cells. In fact, GDVII strain, which does not grow in J774-1 cells (Obuchi et al., 1997), also had a rescue of the growth activity in L*/J774/6 cells (data not shown). As described elsewhere (Obuchi et al., 1997), DA strain infects and actively replicates in J774-1 cells, with only a minimal damage on these cells. This property is clearly important to set the stage for a persistent infection of DA strain in macrophages in vivo. Therefore, DA strain may be able to maintain its genome in macrophages in the presence of L* protein, leading to virus persistence and consequently to demyelination.

As shown in Fig. 4A and B, L* protein had no effects on viral RNA replication and viral protein translation. These results differ from our previous reports (Takata et al., 1998; Obuchi et al., 1999, 2000) that suggested that L* protein probably interferes with viral RNA replication, however, only two time-points (3 and 9 h p.i.) were examined in these previous studies. No effects of L* protein on virus attachment were found in a previous report (Obuchi et al., 1999). As shown in Fig. 3, the titers of cell-associated virus almost paralleled those of cell-free virus in all cells, strongly suggesting that the release of virions are not influenced by the presence or the absence of L* protein. Therefore, L* protein may have some effect(s) on the step of virion assembly. The effect of L* protein is presumably in *trans*.

The formation of viral particles of picornaviruses is reported to be coupled to RNA replication, both events occurring on the surface of virus-induced membranous vesicles found in the cytoplasm of infected cells (Blondel et al., 1998). The poliovirus-induced vesicles are formed closely related on the surface of intracellular membranes, such as the endoplasmic reticulum (ER) (Suhy et al., 2000). Proteins of the poliovirus replication complex, especially 2BC and 3A, accumulate in patches on the ER. Double membrane vesicles derive from the ER (Suhy et al., 2000). Microtubules are known to be closely associated with the ER (Lodish et al., 1995). It may be that the association of L* protein with microtubules is important in TMEV assembly in J774-1 cells or other macrophage cell lines. Of interest, the importance of L* protein to DA growth is not observed in other types of cells (Obuchi et al., 1999). Some unknown host cell factor(s) may have a key interaction with L* protein that is important for virus growth. This may foster DA persistence in a cell key to carrying out DA-induced demyelination. Two-hybrid system may identify this factor(s), and the study is under progress. The restricted growth and persistence of TMEV in macrophages may be critical to the white matter disease. Therefore, the identification of this factor(s) interacting with L* protein may clarify the mechanism(s) of TMEV-induced demyelinating disease.

Acknowledgements

This work was supported by a Grant-in-Aid for Scientific Research from the Ministry of Education, Science, Sports and Culture; and a Grant for Project Research from High-Technology Center of Kanazawa Medical University (H2002-7) and a Grant for Promoted Research from Kanazawa Medical University (S2003-5).

References

Blondel, B., Duncan, G., Couderc, T., Delpeyroux, F., Pavio, N., Colbere-Garapin, F., 1998. Molecular aspects of poliovirus biology with a special focus on the interactions with nerve cells. J. NeuroVirol. 4, 1–26.

Chen, H.-H., Kong, W.-P., Zhang, L., Ward, P.L., Roos, R.P., 1995. A picornaviral protein synthesized out of frame with the polyprotein plays a key role in a virus-induced immune-mediated demyelinating disease. Nat. Med. 1, 927–931.

Ghadge, G.D., Ma, L., Sato, S., Kim, J., Roos, R.P., 1998. A protein critical for a Theiler's virus-induced immune system-mediated demyelinating disease has a cell type-specific antiapoptotic effect and a key role in virus persistence. J. Virol. 72, 8605–8612.

Kong, W.-P., Roos, R.P., 1991. Alternative translation initiation site in the DA strain of Theiler's murine encephalomyelitis virus. J. Virol. 65, 3395–3399.

Lipton, H.L., Jelachich, M.L., 1997. Molecular pathogenesis of Theiler's murine encephalomyelitis virus-induced demyelinating disease in mice. Intervirology 40, 143–152.

Lodish, H., Baltimore, D., Berk, A., Zipursky, S.L., Matsudaira, P., Darnell, J., 1995. Microtubules and intermediate filaments. In: Lodish, H., Baltimore, D., Berk, A., Zipursky, S.L., Matsudaira, P., Darnell, J. (Eds.), Molocular cell biology, third ed. Scientific American books, New York, pp. 1072–1075.

Michiels, T., Jarousse, N., Brahic, M., 1995. Analysis of the leader and capsid coding regions of persistent and neurovirulent strains of Theiler's virus. Virology 214, 550–558.

Miyoshi, H., Takahashi, M., Gage, F.H., Verma, I.M., 1997. Stable and efficient gene transfer into the retina using an HIV-based lentiviral vector. Proc. Natl. Acad. Sci. U.S.A. 94, 10319–10323.

Miyoshi, H., Blömer, U., Takahashi, M., Gage, F.H., Verma, I.M., 1998. Development of a self-inactivating lentivirus vector. J. Virol. 72, 8150–8157.

Naldini, L., Blömer, U., Gallay, P., Ory, D., Mulligan, R., Gage, F.H., Verma, I.M., Trono, D., 1996. In vivo gene delivery and stable transduction of nondividing cells by a lentiviral vector. Science 272, 263–267.

Obuchi, M., Ohara, Y., Takegami, T., Murayama, T., Takada, H., Iizuka, H., 1997. Theiler's murine encephalomyelitis virus subgroup strain-specific infection in a murine macrophage-like cell line. J. Virol. 71, 729–733.

Obuchi, M., Ohara, Y., 1998. Theiler's murine encephalomyelitis virus and mechanisms of its persistence. Neuropathology 18, 13–18.

Obuchi, M., Yamamoto, J., Uddin, M.N., Odagiri, T., Iizuka, H., Ohara, Y., 1999. Theiler's murine encephalomyelitis virus (TMEV) subgroup strain-specific infection in neural and non-neural cell lines. Microbiol. Immunol. 43, 885–892.

Obuchi, M., Yamamoto, J., Odagiri, T., Uddin, M.N., Iizuka, H., Ohara, Y., 2000. L* protein of Theiler's murine encephalomyelitis virus is required for virus growth in a murine macrophage-like cell line. J. Virol. 74, 4898–4901.

Obuchi, M., Odagiri, T., Asakura, K., Ohara, Y., 2001. Association of L* protein of Theiler's murine encephalomyelitis virus with microtubules in infected cells. Virology 289, 95–102.

Ohara, Y., Roos, R.P., 1987. The antibody response in Theiler's virus infection: new perspectives on multiple sclerosis. Prog. Med. Virol. 34, 156–179.

Ohara, Y., Stein, S., Fu, J., Stillman, L., Klaman, L., Roos, R.P., 1988. Molecular cloning and sequence determination of DA strain of Theiler's murine encephalomyelitis viruses. Virology 164, 245–255.

Ralph, P., Prichard, J., Cohn, M., 1975. Reticulum cell sarcoma: An effector cell in antibody-dependent cell-mediated immunity. J. Immunol. 114, 898–905.

Roos, R.P., Stein, S., Ohara, Y., Fu, J., Semler, B.L., 1989. Infectious cDNA clones of the DA strain of Theiler's murine encephalomyelitis virus. J. Virol. 63, 5492–5496.

Roos, R.P., 2002. Pathogenesis of Theiler's murine encephalomyelitis virus-induced disease. In: Semler, B.L., Wimmer, E. (Eds.), Molecular Biology of Picornaviruses. ASM Press, Washington, DC, pp. 427–435.

Sambrook, J., Russell, D.W., 2001. Alternative protocol: high-efficiency calcium-phosphate-mediated transfection of eukaryotic cells with plasmid DNAs, third ed. In: Sambrook, J., Russell, D.W. (Eds.), Molecular Cloning: A Laboratory Manual, vol. 3. Cold Spring Harbor Laboratory Press, Cold Spring Harbor, New York, pp. 16.19–16.20.

Suhy, D.A., Giddings Jr., T.H., Kirkegaard, K., 2000. Remodeling the endoplasmic reticulum by poliovirus infection and by individual viral proteins: an autophagy-like origin for virus-induced vesicles. J. Virol. 74, 8953–8965.

Takata, H., Obuchi, M., Yamamoto, J., Odagiri, T., Roos, R.P., Iizuka, H., Ohara, Y., 1998. L* protein of DA strain of Theiler's murine encephalomyelitis virus is important for virus growth in a murine macrophage-like cell line. J. Virol. 72, 4950–4955.

van Eyll, O., Michiels, T., 2000. Influence of the Theiler's virus L* protein on macrophage infection, viral persistence, and neurovirulence. J. Virol. 74, 9071–9077.

van Eyll, O., Michiels, T., 2002. Non-AUG-initiated internal translation of the L* protein of Theiler's virus and importance of this protein for viral persistence. J. Virol. 76, 10665–10673.

脳機能障害とミクログリアのかかわりおよび細胞を用いた標的化治療・診断

Involvement in the neural dysfunctions and possible therapeutic approach with microglia

鈴木弘美(写真)　澤田　誠
Hiromi Suzuki and Makoto Sawada
藤田保健衛生大学総合医科学研究所

◎脳のマクロファージといわれているミクログリアは脳疾患発症において中心的な役割を果たすと考えられているが，実体は明らかでない．著者らは，ミクログリアがマクロファージと異なり脳に特異的な種々の性質があること，性質の異なるサブタイプが存在していること，神経幹細胞の分化や増殖にも関与することなどを明らかにしてきた．さらに著者らは，ミクログリアを血管に注入すると脳特異的に侵入する能力があることを発見した．そこで，外来性の標識化したミクログリアを脳特異的に非侵襲的に導入する方法を独自に開発し，神経細胞の変性や脳機能障害におけるミクログリアの役割や動態をバイオイメージングの手法を取り入れるなどして調べた．また，この脳特異的細胞導入を応用することにより，脳疾患における神経細胞の変性や脳機能障害に対する新しい治療法についても検討した．この性質の研究は脳の疾患発症のメカニズム解明だけでなく，新しい標的化治療・診断法の開発にもつながると考えられる．

Key word：ミクログリア，サブタイプ，ドラッグデリバリーシステム，遺伝子治療

ミクログリアの脳特異的侵入

ミクログリアはマクロファージ様の中枢神経系細胞で，炎症反応やウイルス感染において免疫担当細胞として働いたり，変性した細胞を取り除く貪食細胞として働くほか，脳内サイトカインネットワークの中心的な細胞である[1]．これまでミクログリアの起源は周産期に脳内に侵入した単球が特殊化して分化すると考えられてきた．しかし，最近の著者らの研究から，マクロファージ欠損マウス脳に正常とほぼ同数のミクログリアが存在することや，ミクログリアが骨髄で造血が起こるより早い発生の段階から脳内に存在することが明らかとなり，ミクログリアは骨髄で分化したマクロファージとは異なる細胞起源をもつと考えられる．さらに著者らは，脳に対する親和性や脳に浸潤できるかどうかについて調べ，マクロファージとミクログリアが決定的に異なることを示した[2]．

脳は血液脳関門が存在するため，末梢からの物質や細胞の浸潤がほとんどなく，薬物や遺伝子導入が困難である．実際に正常脳ではT細胞やマクロファージなどの免疫細胞の浸潤はほとんどみられない．そこで，それぞれの細胞を精製単離して蛍光標識を施した後，マウス個体に血管内投与してみた．このときマクロファージは末梢臓器には移行性がみられるものの脳にはほとんど集積しなかった．しかし，ミクログリアは末梢臓器にはほとんど移行せず，脳に特異的に集積した[3]．この性質を利用して精製ミクログリアに外来遺伝子を導入し，これを末梢血管投与することで，脳に目的遺伝子を発現させることができるようになった[4]．また，GFP恒常的発現ミクログリアを導入した場合，導入後数カ月にわたって脳内にGFP陽性ミク